CDF note 9092

Measurement of CP-violating asymmetries and of branching fractions of $\Lambda_b^0 \to p\pi^-$ and $\Lambda_b^0 \to pK^-$ decays

The CDF Collaboration
URL http://www-cdf.fnal.gov

(Dated: January 9, 2008)

Using 1 fb^{-1} of two-track trigger data collected by the upgraded Collider Detector at the Fermilab Tevatron, we report the first branching ratio measurement of hadronic charmless Λ_b^0 decays:

$$\frac{\sigma(p\bar{p} \to \Lambda_b^0 X, p_T > 6 \text{ GeV/c})}{\sigma(p\bar{p} \to B^0 X, p_T > 6 \text{ GeV/c})} \frac{\mathcal{B}(\Lambda_b^0 \to p\pi^-)}{\mathcal{B}(B^0 \to K^+\pi^-)} = 0.0415 \pm 0.0074 \; (stat.) \pm 0.0058 \; (syst.)$$

$$\frac{\sigma(p\bar{p} \to \Lambda_b^0 X, p_T > 6 \text{ GeV/c})}{\sigma(p\bar{p} \to B^0 X, p_T > 6 \text{ GeV/c})} \frac{\mathcal{B}(\Lambda_b^0 \to pK^-)}{\mathcal{B}(B^0 \to K^+\pi^-)} = 0.0663 \pm 0.0089 \; (stat.) \pm 0.0084 \; (syst.)$$

We also report the first measurement of CP-violating asymmetries in these decays:

$$A_{\mathsf{CP}}(\Lambda_b^0 \to p\pi^-) = 0.03 \pm 0.17 \; (stat.) \pm 0.05 \; (syst.)$$

$$A_{\mathsf{CP}}(\Lambda_b^0 \to pK^-) = 0.37 \pm 0.17 \; (stat.) \pm 0.03 \; (syst.).$$

Preliminary results approved October 18, 2007

I. INTRODUCTION

The investigation of CP-violating decay-rate asymmetries of b-flavored hadrons provides useful insight into the flavor sector of the Standard Model. Experimentally, CP asymmetries have been observed in B^0 and B^+ decays, and the first indications are becoming available these days for B^0_s decays. On the other hand, no asymmetry has yet been measured in baryon decays, available in much smaller samples.

Two-body charmless Λ^0_b decays into self-tagging final states with a proton and a charged pion (or kaon) are promising for studying CP-violating asymmetries, which may reach significant size $\mathcal{O}(10\%)$ in the Standard Model [1], thus being experimentally more accessible. The presence of interfering strong phases, necessary to make the direct asymmetries observable, complicates the theoretical interpretation of the experimental results. However, measurements of asymmetries and of (as yet unknown) branching fractions, are believed to be potentially useful to rule out, or allow, some extensions of the Standard Model. Mohanta, for instance, shows in [2], that Minimal Supersymmetric Extensions of the Standard Model in which the R-parity is violated could both strongly suppress asymmetries in charmless Λ^0_b decays and enhance by factors $\mathcal{O}(100)$ their branching fractions with respect to the Standard Model predictions. This makes the measurement of these quantities particularly suited to increase our information on possible new physics scenarios before the LHC will begin its operations.

CDF is currently the only experiment able to collect and reconstruct such decays. The CDF II detector is a solenoidal magnetic spectrometer surrounded by 4π calorimeters and muon detectors. Particle identification is provided by the measurement of the specific ionization energy-loss in the drift chamber and by a scintillator-based time-of-flight detector. More details on the CDF II detector can be found in Ref. [3] and in references therein.

In 2005, a 2.3×10^-5 upper limit for the sum of branching fractions of $\Lambda^0_b \to p\pi^-$ and $\Lambda^0_b \to pK^-$ decays, using 180 pb^{-1} of data waspublished [4]. More recently, and with a larger 1 fb^{-1} sample, we obtained the first observation of these decays [5], in the context of the $B^0_{(s)} \to h^+h^{'-}$ analysis, in which they were considered as backgrounds. We describe here a dedicated analysis aimed at the first measurement of CP-violating asymmetries and branching fraction in such decays [6].

A large fraction of this analysis is common to the $B^0_{(s)} \to h^+h^{'-}$ analysis, whose corresponding public document can be consulted for further details [5]. Throughout this document, C-conjugate modes are implied and branching fractions indicate CP-averages unless otherwise stated. Figures and plot of this analysis can be found in `www-cdf.fnal.gov/physics/new/bottom/071018.blessed-Lbph`

II. DATA SAMPLE AND EVENT SELECTION

We analyzed a $\int \mathcal{L}dt \simeq 1$ fb^{-1} sample of pairs of oppositely-charged particles, used to form b-hadron (i.e. B^0, B^0_s, and Λ^0_b) candidates, with $p_T > 2$ GeV/c and $p_T(1) + p_T(2) > 5.5$ GeV/c. The trigger required also a transverse opening-angle between tracks $20^\circ < \Delta\phi < 135^\circ$ to reject background from particles within light-quark jets [7]. In addition, both charged particles were required to originate in a displaced vertex ($100\ \mu$m $< d_0 < 1$ mm), while the b-hadron candidate was required to be produced in the primary p$\bar{\text{p}}$ interaction ($d_0(B) < 140\ \mu$m) and to have traveled a transverse distance $L_{xy}(B) > 200\ \mu$m.

A $B^0_{(s)} \to h^+h^{'-}$ signal of about 14500 events and signal-to-noise ratio SNR $\simeq 0.2$ (at the peak) is visible in data (see Fig. 1) already after confirming the trigger selection on offline quantities. The extraction of a visible $\mathcal{B} \simeq 10^{-5}$ signal at trigger-level is a remarkable achievement at a hadron collider, made it possible by the CDF trigger on displaced tracks [8].

In the offline analysis, an unbiased procedure of optimization determined a tightened selection on track-pairs fit to a common decay-vertex. For this analysis, we chose the selection cuts by minimizing the expected uncertainty individually for each of the physical observables to be measured. The uncertainty on such observables has been parameterized with analytical functions of the signal yield (S) and background level (B). The free parameters of these functions were determined from analysis of pseudo-experiments reproducing the experimental circumstance of data.

For each set of cuts, S was estimated from Monte Carlo simulation and normalized to the yield observed in data after the trigger selection, and B is the background extrapolated from the sidebands of the $\pi\pi$-mass distribution in the data. We used the selection optimized for maximizing the sensitivity for discovery and limit setting of rare modes such as $B^0_s \to K^-\pi^+$ or $\Lambda^0_b \to p\pi^-$ and $\Lambda^0_b \to pK^-$ decays [9] (Tab. I). This approach led to an improvement in average expected statistical resolution on the yield of a new signal with respect to the case in which the usual $\sqrt{\text{S}+\text{B}}/\text{S}$ score function is used. Besides tightening the trigger cuts, in the offline analysis the discriminating power of the $B^0_{(s)}$ meson 'isolation' and the information provided by the 3D reconstruction capability of CDF tracking have been used to obtain a great improvement in signal purity. Isolation is defined as $I(B) = p_{\text{T}}(B)/[p_{\text{T}}(B) + \sum_i p_{\text{T}}(i)]$, in which the sum runs over every other track within a cone of radius one in the $\eta - \phi$ space around the $B^0_{(s)}$ meson flight-direction. By requiring $I(B) > 0.525$ in addition to the trigger cuts (Tab. I), we reduced the background by a factor four while keeping almost 80% of signal. The 3D view of tracking ($\chi^2_{3D}(B)$) allowed to resolve multiple vertices along the beam direction, thus reducing the background (mainly pairs of displaced tracks coming from distinct, uncorrelated heavy-flavor decays) by a factor two, with a small inefficiency on the signal. An additional requirement on the transverse momentum of b-hadron candidates ($p_{\mathrm{T}}(B) > 6$ GeV/c) is needed because the Λ^0_b spectrum, a necessary input to simulation for the extraction of efficiencies and fit templates, has been measured in CDF Run II data only above that threshold. The resulting $\pi\pi$-mass distribution (see Fig. 2, left plot) shows a clean signal of $B^0_{(s)} \to h^+h^{'-}$ decays (centered approximately at $m_{\pi\pi} = 5.25$ GeV/c^2) accompanied by a smaller, but evident, contribution in the high-mass side of the main peak ($m_{\pi\pi} = 5.45$ GeV/c^2). A simple estimate of event yields with a binned one-dimensional fit with a Gaussian (signal) plus an Exponential (combinatoric background) and an Argus-shaped (physical background) function yields 3966 ± 70 events, with standard deviation $\sigma = 40 \pm 0.7$ MeV/c^2 and SNR $\simeq 15$ at peak. In spite of the good CDF mass resolution ($\simeq$22 MeV/c^2), the different decays overlap into an unresolved mass peak, as also expected by Monte Carlo simulations (Fig. 2, right plot). Contributions to the peak include modes already established $B^0 \to \pi^+\pi^-$, $B^0 \to K^+\pi^-$, $B^0_s \to K^+K^-$ and rarer modes such as $B^0 \to K^+K^-$, $B^0_s \to K^-\pi^+$, $B^0_s \to \pi^+\pi^-$, $\Lambda^0_b \to p\pi^-$, $\Lambda^0_b \to pK^-$. Also the PID resolution is insufficient for separating them on an event-by-event basis, we therefore aimed at a statistical separation, by using a multivariate, unbinned, maximum-likelihood fit (fit of composition) that exploits PID information (provided by the dE/dx in the drift chamber) and kinematics. The goal of this analysis is to precisely measure the fraction of the individual Λ^0_b decay modes with respect to a reference mode. We chose the $B^0 \to K^+\pi^-$ as reference since it is the more abundant in our sample (thus introducing the smallest statistical uncertainty in the ratio of fractions) and its branching fraction is accurately known from B-factories measurements [10].

III. FIT OF COMPOSITION

The fit of composition allows to statistically determine the fraction of each mode with respect to the global signal, and to measure the CP-violating asymmetries of the self-tagging modes (those that have different particles in their final states), including Λ^0_b decays into proton-kaon, or proton-pion final states. For the kinematic portion, we exploit the correlation between invariant mass, ratio of momenta and charge, to construct three loosely correlated observables that contain in a compact form the full information carried by all possible values of invariant mass of the candidate b-hadron, resulting from different mass assignments to the two outgoing particles. They are a) the mass $m_{\pi\pi}$ calculated with the pion mass assignment to both particles; b) the signed momentum imbalance $\alpha = (1 - p_1/p_2)q_1$, where p_1 (p_2) is the lower (higher) of the particle momenta, and q_1 is the sign of the charge of the particle of momentum p_1; c) the scalar sum of the particle momenta $p_{\mathrm{tot}} = p_1 + p_2$. The mass of any particular mode m_{12} ($m_{K\pi}, m_{\pi K}, m_{KK}, m_{p\pi}, m_{\pi p}, m_{pK}, m_{Kp}$) can be expressed as

$$m^2_{12} = m^2_{\pi\pi} - 2m^2_\pi + (m^2_1 + m^2_2) - 2 \cdot \left(\sqrt{p^2_1 + m^2_\pi} \cdot \sqrt{p^2_2 + m^2_\pi} - \sqrt{p^2_1 + m^2_1} \cdot \sqrt{p^2_2 + m^2_2}\right), \tag{1}$$

$$\text{with } p_1 = \frac{1 - |\alpha|}{2 - |\alpha|} p_{\mathrm{tot}} \qquad p_2 = \frac{1}{2 - |\alpha|} p_{\mathrm{tot}}, \tag{2}$$

where m_1 (m_2) is the mass of the lower (higher) momentum particle. For simplicity the Eq. 1 is written as function of p_1 and p_2 instead of α and p_{tot}. The separation power of this kinematic parameterization is visible in the scatter-plot of the invariant $\pi\pi$-mass, $m_{\pi\pi}$, as a function of α (Figs. 3,4,5) or better in the two-dimensional distribution of averaged $m_{\pi\pi}$ as a function of α (Fig. 6). The p_{tot} observable does not provide significant separation but it plays a key rôle in accounting for the dependence of the particle identification observables on particle momentum: p_{tot} in conjunction with α provides unique identification of the momenta of both particles. Particle identification (PID) information is summarized by a single observable ID for each track defined as

$$\mathsf{ID}(\text{track}) = \frac{\left.\frac{\mathrm{dE}}{\mathrm{dx}}\right|_{\mathrm{meas}}(\text{track}) - \left.\frac{\mathrm{dE}}{\mathrm{dx}}\right|_{\pi}(\text{track})}{\left.\frac{\mathrm{dE}}{\mathrm{dx}}\right|_{\mathrm{K}}(\text{track}) - \left.\frac{\mathrm{dE}}{\mathrm{dx}}\right|_{\pi}(\text{track})}, \tag{3}$$

where the $dE/dx|_{meas}$ is the measured specific ionization energy loss by the charged particle in the drift chamber and the $dE/dx|_{\pi(K)}$ is the expected value for this quantity in a given particle hypothesis, i.e. π, K, or p given the particle momentum. Since kaons and pions are the most abundant particles in our sample, use of the ID observable is convenient since its average, in pion and kaon particle hypothesis, is $<\mathsf{ID}>_\pi = 0$ and $<\mathsf{ID}>_K = 1$, respectively – and independent of momenta to a large approximation. The likelihood contribution of the i^{th} event is written as

$$\mathcal{L}_i = (1-b)\sum_j f_j \mathcal{L}_j^{\rm kin}\mathcal{L}_j^{\rm PID} + b\left(f_{\rm A}\mathcal{L}_{\rm A}^{\rm kin}\mathcal{L}_{\rm A}^{\rm PID} + (1-f_{\rm A})\mathcal{L}_{\rm E}^{\rm kin}\mathcal{L}_{\rm E}^{\rm PID}\right), \quad (4)$$

where

$$\mathcal{L}_j^{\rm kin} = R(m_{\pi\pi} - \mathcal{M}_j(\alpha, p_{\rm tot}), \alpha, p_{\rm tot})P_j(\alpha, p_{\rm tot}), \quad (5)$$

$$\mathcal{L}_{\rm A}^{\rm kin} = {\rm Argus}(m_{\pi\pi}|c_2, m_0)P_{\rm A}(\alpha, p_{\rm tot}), \quad (6)$$

$$\mathcal{L}_{\rm E}^{\rm kin} = e^{c_1 m_{\pi\pi}}P_{\rm E}(\alpha, p_{\rm tot}), \quad (7)$$

$$\mathcal{L}_{j({\rm E,A})}^{\rm PID} = F_{j({\rm E,A})}(\mathsf{ID}_1, p_1(\alpha, p_{\rm tot}), \mathsf{ID}_2, p_2(\alpha, p_{\rm tot})). \quad (8)$$

The index 'A(E)' labels the combinatorial(physical) background-related quantities, the index j runs over the twelve distinguishable $B^0_{(s)} \to h^+h^{'-}$ and $\Lambda^0_b \to ph^-$ modes (Fig. 6), and f_j are their fractions, to be determined by the fit together with the total background fraction b and with the fraction of the physical(combinatorial) background $f_{A(E)}$. The conditional probability density $R(m_{\pi\pi} - \mathcal{M}_j(\alpha, p_{\rm tot}), \alpha, p_{\rm tot})$ is the mass resolution function of each mode j when the correct mass is assigned to both tracks. In fact the average mass $\mathcal{M}_j(\alpha, p_{\rm tot})$ is the value of $m_{\pi\pi}$ obtained from Eq. (1) by setting the appropriate particle mass for each decay mode j. With a variable-change we obtain $R(m_{\pi\pi} - \mathcal{M}_j(\alpha, p_{\rm tot}), \alpha, p_{\rm tot}) = R(M_j - M_{B^0(B^0_s,\Lambda^0_b)}, \alpha, p_{\rm tot})$ where M_j is the invariant mass computed with the correct mass assignment to both particles for each mode j. The resolution function (R) was parameterized with an accurate study using the detailed CDF II simulation. To account for non-Gaussian tails due to the emission of photons in the final state (FSR) we modified "ad hoc" the CDF II simulation and we introduced the soft photon emission following recent QED calculations [11]. The width of the mass resolution function is momentum-dependent and the dependences by α and $p_{\rm tot}$ are included in the fit. The dominant Gaussian (about 85% of the total) has an average width $\sigma_{\alpha,p_{\rm tot}} \simeq 22$ MeV$/c^2$.
We checked the reliability of the mass resolution model using 1.5×10^6 $D^{*+} \to D^0(\to K^-\pi^+)\pi^+$ decays (Fig. 17) and fitting the mass line shape of the $D^0 \to K^-\pi^+$ peak, where the signal function was completely fixed from the model, while the background function was free to vary (straight line) obtaining a very good agreement between data and simulation.
We used the B^0, B^0_s, and Λ^0_b masses measured by CDF [12] to cancel the common systematic uncertainty. The background mass distribution is determined in the fit by varying the parameters c_1, c_2 and m_0 in Eq. (6,7). The $P_j(\alpha, p_{\rm tot})$ is the joint probability distribution of $(\alpha, p_{\rm tot})$, and is parameterized for each mode j with Chebychev polynomials (Figs. 7–14) fitted to Monte Carlo samples produced by a detailed detector simulation. The background function $P_{\rm A(E)}$ is obtained from the mass sidebands of data. The same sample of D^{*+} decays used to study the mass line-shape, where the D^0 decay products are identified by the charge of the D^{*+} pion, was used to calibrate the dE/dx response over the tracking volume and time, and to determine the F functions in (8) [13]. The $\mathcal{O}(0.4\%)$ contamination from doubly Cabibbo-suppressed $D^0 \to K^+\pi^-$ decays was neglected. In a $> 95\%$ pure D^0 sample, we obtained a momentum-independent 1.5σ separation between kaons and pions (Fig. 18), corresponding to an uncertainty on the measured fraction of each class of particles that is just 60% worse than the uncertainty attainable with ideal separation. We measured a 10% residual track-to-track correlation due to common-mode dE/dx fluctuations and since the correlation is sample dependent we fitted in the fit of composition the dE/dx correlation of the $B^0_{(s)} \to h^+h^{'-}$ modes using a sum of two Gaussian.

The background term in (8) is similar to the signal terms, but allows for independent pion, kaon, proton, and electron components, which are free to vary independently. Muons are indistinguishable from pions with the available dE/dx resolution.

IV. FIT RESULTS

The fits returned the fractions and the yields listed in Tab. II. Secondary fit results are reported in Tab. III. Significant signals were seen for all modes, $B^0 \to \pi^+\pi^-$, $B^0 \to K^+\pi^-$, $B^0_s \to K^+K^-$, $B^0_s \to K^-\pi^+$, $\Lambda^0_b \to p\pi^-$ and $\Lambda^0_b \to pK^-$ previously observed in this same sample in the context of the $B^0_{(s)} \to h^+h^{'-}$ analysis [5]. In order to visualize the agreement between the fit and the data, we reported the plots of the fit projections. The relevant projections are those onto the fit observables $m_{\pi\pi}$, α, $p_{\rm tot}$, $\mathsf{ID}(1)$ and $\mathsf{ID}(2)$ and other two additional PID observables (linear combination of ID_1 and ID_2) $\mathsf{ID}_{\rm sum} = \mathsf{ID}_1 + \mathsf{ID}_2$ and $\mathsf{ID}_{\rm dif} = \mathsf{ID}_1 - \mathsf{ID}_2$ (Figs. 19–22). An alternative way to check the goodness of the fit of composition and to visualize the separation power between the different modes is the "*relative likelihood*" plot (Figs. 23–24). The agreement between data and fit function is very satisfactory.

To convert raw yields into relative branching fractions, we applied corrections for the different detector acceptances and for different trigger and offline selection efficiencies among the different decay modes. For the measurement of the CP-violating asymmetry, the $\Lambda_b^0 \to p\pi^-$ ($\Lambda_b^0 \to pK^-$) and $\overline{\Lambda}_b^0 \to \overline{p}\pi^+$ ($\overline{\Lambda}_b^0 \to \overline{p}K^+$) yields are corrected for the different probability of interaction in matter between positive and negative pions, kaons, and protons. We used a sample of $1\,\mathrm{fb}^1$ $\Lambda^0 \to p\pi$ decays to determine from data the efficiency ratios $\varepsilon(p\pi^-)/\varepsilon(\overline{p}\pi^+)$ and $\varepsilon(pK^-)/\varepsilon(\overline{p}K^+)$. The kinematic features of this sample in our trigger allow to unambiguously distinguish Λ^0 from $\bar{\Lambda}^0$ decays only by evaluating the invariant mass under the hypothesis that the momentum of the proton is always greater than the pion's (kaon's) one. Assuming equal production rate of Λ^0 and $\bar{\Lambda}^0$ with zero CP-violating asymmetry, any residual asymmetry in the relative yield of Λ^0 and $\bar{\Lambda}^0$ is induced by the detector-reconstruction code. The corrections are found to be smaller than $\mathcal{O}(2\%)$ and were checked against variations as a function of polar or azimuthal angle of the Λ^0 and of its displacement from the primary vertex. For the measurement of the $\Lambda_b^0 \to p\pi^-$ and $\Lambda_b^0 \to pK^-$ branching fractions relative to the reference $B^0 \to K^+\pi^-$ mode, we corrected for a number of effects including different kinematics, different lifetime, different transverse-momentum spectra etc. These corrections were determined from the detailed detector simulation with the following exception evaluated using real data. The lower specific ionization of kaons with respect to pions in the drift chamber is responsible for a $\simeq 5\%$ lower efficiency to reconstruct a kaon by the XFT. This effect was measured in a sample of $D^+ \to K^-\pi^+\pi^+$ decays triggered on two tracks, using the unbiased third track. Since the ionization of protons in the desired momentum range is very similar to the one of kaon we extended this correction to the protons and assigned a conservative systematic uncertainty. The possible differences in efficiency of the isolation requirement between the Λ_b^0 and the B^0 meson (of the reference mode) are taken into account with a conservative systematic uncertainty.

V. SYSTEMATIC UNCERTAINTIES

All systematics uncertainties are smaller than the statistical ones. Their are listed in the Tab. IV. A short explanation follows.

- *Mass scale.* The central fit is performed by assuming a known global mass scale, in which we assign to the B^0, B_s^0 and Λ_b^0 masses the values measured in CDF Run II [12]. Since the mass is used in separating the different contributions it is interesting to check how the fit behaves when the mass scale is allowed to float. An additional output parameter Δ was added to the fit in the parameterization of the input masses: $m_{B_s^0}^{\mathrm{fit}} = m_{B_s^0}^{\mathrm{CDFII}} + \Delta$, $m_{B^0}^{\mathrm{fit}} = m_{B^0}^{\mathrm{CDFII}} + \Delta$ and $m_{\Lambda_b^0}^{\mathrm{fit}} = m_{\Lambda_b^0}^{\mathrm{CDFII}} + \Delta$ and the global scale of masses is determined to be: 1.6 ± 0.8 MeV/c^2. The difference in $-2\ln\mathcal{L}$ between this last fit and the central fit is of four units. Then, we generated an ensemble of pseudo-experiments in which the global mass scale is shifted by the above measured value, and we applied the fit to these toy-MC.

- *Input masses.* The b-hadron masses are an input parameter to the fit through the analytic expressions of $\mathcal{M}_j(\alpha, p_{\mathrm{tot}})$. We generated distinct ensembles of pseudo-experiments in which we independently varied the B^0, B_s^0, and Λ_b^0, input masses within $\pm1\sigma$ statistical uncertainty of the published CDF Run II measurement [12] to evaluate the systematics due to the uncertainty on the input masses.

- *dE/dx induced systematics.* We repeated the global fit on pseudo-experiments in which the PID templates were generated by randomly varying the several parameters associated to dE/dx calibrations within a 1σ-radius multidimensional sphere.

- *Combinatorial-background model:* The central fit uses a straight-line distribution function for the combinatorial background. We repeated the fit on large ensembles of pseudo-experiments using polynomial distributions (second degree maximum) and exponential functions for the combinatorial background.

- *Effect of Λ_b^0 polarization:* In the central fit we assumed no polarization for the Λ_b^0. In case that hadroproduced Λ_b^0 have non-zero polarization, the kinematics of the decay would change thus altering the acceptances and making inaccurate the parameterization of the momentum p.d.f. We first fitted on data the possible polarization in our sample, assuming the (non-relativistic) worst-case in which the angular distribution of a final state particle from decays of fully polarized Λ_b^0 assumes the form $dN/d\cos(\theta^*) \propto f_\pm(\theta^*) = 1 \pm \cos(\theta^*)$, as a function of the polar angle in the center-of-mass reference frame. The fit yielded $\mathcal{P} = 0.55 \pm 0.18$ to be compared to $\mathcal{P} = 0.5$ in case of unpolarized baryons. Similarly, no polarization-asymmetry is measured between Λ_b^0 and $\bar{\Lambda}_b^0$ baryon. The measured asymmetries and relative branching ratios vary very little with respect to the central fit. We used the results of this fit to produce 200 pseudo-experiments in which Λ_b^0 (and $\bar{\Lambda}_b^0$) were generated with polarizations ranging from $\mathcal{P}_+ = 0.55 + 0.18 = 0.73$ to $\mathcal{P}_- = 0.55 - 0.18 = 0.37$. These pseudo-experiments were fit using the likelihood of our central fit (that assumes $\mathcal{P} = 0.5$) and the difference in fit results were quoted as systematic uncertainty.

- *Detector-induced charge asymmetries.* The statistical uncertainty on the determination of the detector-induced charge asymmetries propagates as a systematic uncertainty on the measurement of the asymmetries. However we also considered a further source of systematic, arising from the limitations of the evaluation on data of these asymmetries. In fact, as a cross-check, we compared the charge-asymmetries extracted from data with the same quantities extracted from simulated samples. Discrepancies of order 5% are observed and can be ascribed to several causes, e.g. the fact that Λ^0 used to extract the corrections have spin and their production is polarized. If their polarization is different from the (unknown) Λ_b^0 polarization, the corrections extracted from data may be inaccurate. Therefore, while still using real data for our central result, we use the difference between central values from data-based correction and from simulation-based correction as a systematics.

- *Lifetime induced systematics.* The Λ_b^0 lifetime is known with $\approx 6\%$ uncertainty. This propagates as an uncertainty in acceptance and in the shape of kinematic templates in our measurement of the relative branching fractions. We extracted from pseudo-experiments the relevant kinematic parameterizations and expected acceptance and efficiency corrections in case of Λ_b^0 lifetimes increased or decreased by one standard deviation in either side of the central value. The maximum difference is quoted as a systematic uncertainty.

- *Uncertainties in momentum distributions.* Possible discrepancies between the actual Λ_b^0 spectrum and the one used in our simulation to extract fit templates and efficiencies may be hidden by the currently low statistics of Λ_b^0 in data. We therefore estimated a systematic uncertainty on the poor knowledge of the Λ_b^0 spectrum by conservatively assuming that the $b-$hadron spectrum measured by CDF Run II is entirely dominated by Λ_b^0 and repeating the measurement under this assumption. The (tiny) difference between the obtained fit results and those of the central fit (in which the Λ_b^0 spectrum is reweighted according to the spectrum measured in the $\Lambda_b^0 \to \Lambda_c^0 \pi$ analysis) is taken as systematics uncertainty.

  An additional cross-check was done by increasing the degrees of freedom in fitting the momentum templates ($p(\alpha, p_{\rm tot})$), and allowing asymmetric α-distributions also for modes with kinematically symmetric (i.e. two particles with equal mass) final states. No difference was observed in the fit results.

- *Uncertainties on isolation cut efficiency and drift-chamber track trigger efficiency.* The dominant systematic uncertainty arise from the poor knowledge of the isolation distributions of Λ_b^0 and of the difference in probability for a proton to trigger the drift-chamber track trigger with respect to a kaon. The first uncertainty is due to our cut on the isolation variable, whose distribution is known for B^0 mesons but not for Λ_b^0. Based on previous studies on differences in isolations between B^0 and B_s^0 mesons [5], we assumed the efficiency of the isolation cut on Λ_b^0 the same as on B^0 and considered a conservative 10% of statistical uncertainty. Due to their different specific ionization energy loss, protons, kaons and pions have different probabilities of trigger the drift-chamber based track trigger. This difference was found to be $\mathcal{O}(5\%)$ between pions and kaons [5]. Since proton ionization in the momentum range of interest is similar to ionization from kaons, we assumed their trigger efficiency equal assuming a conservative systematic uncertainty of 5%. .

VI. RESULTS

Using 1 fb^{-1} of two-track trigger data we measured the following CP-violating asymmetries:

$$A_{\mathsf{CP}}(\Lambda_b^0 \to p\pi^-) = \frac{\mathcal{B}(\Lambda_b^0 \to p\pi^-) - \mathcal{B}(\overline{\Lambda}_b^0 \to \overline{p}\pi^+)}{\mathcal{B}(\Lambda_b^0 \to p\pi^-) + \mathcal{B}(\overline{\Lambda}_b^0 \to \overline{p}\pi^+)} = 0.03 \pm 0.17\ (stat.) \pm 0.05\ (syst.),$$

$$A_{\mathsf{CP}}(\Lambda_b^0 \to pK^-) = \frac{\mathcal{B}(\Lambda_b^0 \to pK^-) - \mathcal{B}(\overline{\Lambda}_b^0 \to \overline{p}K^+)}{\mathcal{B}(\Lambda_b^0 \to pK^-) + \mathcal{B}(\overline{\Lambda}_b^0 \to \overline{p}K^+)} = 0.37 \pm 0.17\ (stat.) \pm 0.03\ (syst.).$$

This is the first such measurement in b-baryon decays. The statistical uncertainty dominates the resolution and prevents a conclusive statement on the presence of asymmetry, whose measured value deviates from zero at the 2.1σ level in the pK case and is fully consistent with zero in the $p\pi$ case.

In addition, we quote also the following branching ratio measurement relative to a well-known, reference B^0 decay:

$$\frac{\sigma(p\bar{p} \to \Lambda_b^0 X, p_T > 6\ \mathrm{GeV}/c)}{\sigma(p\bar{p} \to B^0 X, p_T > 6\ \mathrm{GeV}/c)} \frac{\mathcal{B}(\Lambda_b^0 \to p\pi^-)}{\mathcal{B}(B^0 \to K^+\pi^-)} = 0.0415 \pm 0.0074\ (stat.) \pm 0.0058\ (syst.)$$

$$\frac{\sigma(p\bar{p} \to \Lambda_b^0 X, p_T > 6\ \mathrm{GeV}/c)}{\sigma(p\bar{p} \to B^0 X, p_T > 6\ \mathrm{GeV}/c)} \frac{\mathcal{B}(\Lambda_b^0 \to pK^-)}{\mathcal{B}(B^0 \to K^+\pi^-)} = 0.0663 \pm 0.0089\ (stat.) \pm 0.0084\ (syst.).$$

VII. DERIVED RESULTS

Our measurement can be combined with another branching fraction measurement performed in CDF Run II [16] to estimate the ratio of branching fractions using the decay $\Lambda_b^0 \to \Lambda_c^+\pi^-$ as reference mode for the Λ_b^0 charmed branching-fraction. Thus, we quote $\frac{\mathcal{B}(\Lambda_b^0 \to p\pi^-)}{\mathcal{B}(\Lambda_b^0 \to \Lambda_c^+\pi^-)}$ and $\frac{\mathcal{B}(\Lambda_b^0 \to pK^-)}{\mathcal{B}(\Lambda_b^0 \to \Lambda_c^+\pi^-)}$ extracted as follows:

$$\frac{\mathcal{B}(\Lambda_b^0 \to p\pi^-)}{\mathcal{B}(\Lambda_b^0 \to \Lambda_c^+\pi^-)} = \frac{f_{\mathrm{baryon}}\mathcal{B}(\Lambda_b^0 \to p\pi^-)}{f_d\mathcal{B}(B^0 \to K^+\pi^-)} \times \frac{f_d\mathcal{B}(B^0 \to D^-\pi^+)}{f_{\mathrm{baryon}}\mathcal{B}(\Lambda_b^0 \to \Lambda_c^+\pi^-)} \times \frac{\mathcal{B}(B^0 \to K^+\pi-)}{\mathcal{B}(B^0 \to D^-\pi^+)},$$

$$\frac{\mathcal{B}(\Lambda_b^0 \to pK^-)}{\mathcal{B}(\Lambda_b^0 \to \Lambda_c^+\pi^-)} = \frac{f_{\mathrm{baryon}}\mathcal{B}(\Lambda_b^0 \to pK^-)}{f_d\mathcal{B}(B^0 \to K^+\pi^-)} \times \frac{f_d\mathcal{B}(B^0 \to D^-\pi^+)}{f_{\mathrm{baryon}}\mathcal{B}(\Lambda_b^0 \to \Lambda_c^+\pi^-)} \times \frac{\mathcal{B}(B^0 \to K^+\pi-)}{\mathcal{B}(B^0 \to D^-\pi^+)},$$

where

- $\frac{f_{\mathrm{baryon}}\mathcal{B}(\Lambda_b^0 \to p\pi^-)}{f_d\mathcal{B}(B^0 \to K^+\pi^-)}$ = and $\frac{f_{\mathrm{baryon}}\mathcal{B}(\Lambda_b^0 \to pK^-)}{f_d\mathcal{B}(B^0 \to K^+\pi^-)}$ are the efficiency-corrected fit results;
- the ratio $\frac{f_{\mathrm{baryon}}\mathcal{B}(\Lambda_b^0 \to \Lambda_c^+\pi^-)}{f_d\mathcal{B}(B^0 \to D^-\pi+)} = 0.82 \pm 0.08(\mathrm{stat.}) \pm 0.11(\mathrm{syst.} \pm 0.22\ (\mathcal{B}_{\Lambda_c^+}))$ is taken from the CDF Run II measurement [16];
- the ratio $\frac{\mathcal{B}(B^0 \to K^+\pi-)}{\mathcal{B}(B^0 \to D^-\pi+)} = \frac{(1.88 \pm 0.07) \times 10^{-5}}{(2.68 \pm 0.13) \times 10^{-3}} = (7.01 \pm 0.43) \times 10^{-3}$ is taken from the PDG [10].

This results in:

$$\frac{\mathcal{B}(\Lambda_b^0 \to p\pi^-)}{\mathcal{B}(\Lambda_b^0 \to \Lambda_c^+\pi^-)} = (0.355 \pm 0.063\ (stat.) \pm 0.080\ (syst.) \pm 0.096\ (\mathcal{B}_{\Lambda_c^+})) \times 10^{-3},$$

$$\frac{\mathcal{B}(\Lambda_b^0 \to pK^-)}{\mathcal{B}(\Lambda_b^0 \to \Lambda_c^+\pi^-)} = (0.567 \pm 0.076\ (stat.) \pm 0.120\ (syst.) \pm 0.150\ (\mathcal{B}_{\Lambda_c^+})) \times 10^{-3}.$$

The relative branching ratio measurements can also be used to extract absolute branching fractions for charmless Λ_b^0 decays using the world average values of ratios of fragmentation functions ($f_{\mathrm{b-baryon}}/f_d = 0.25 \pm 0.04$) and of the $B^0 \to K^+\pi^-$ decay rate, $\mathcal{B}(B^0 \to K^+\pi^-) = (1.82 \pm 0.08) \times 10^{-5}$, [10]:

$$\mathcal{B}(\Lambda_b^0 \to p\pi^-) = (3.1 \pm 0.6\ (stat.) \pm 0.7\ (syst.)) \times 10^{-6},$$

$$\mathcal{B}(\Lambda_b^0 \to pK^-) = (5.0 \pm 0.7\ (stat.) \pm 1.0\ (syst.)) \times 10^{-6}.$$

While for the moment the ratio $f_{\mathrm{b-baryon}}/f_d$ is taken from the PDG (that is, from LEP measurement at the Z^0 pole) we are aware that significantly different values for this ratio may be more appropriate for a measurement at the Tevatron, where we are sensitive to p_{T} of the beauty hadron much lower than those probed at LEP. For this reason we also quote absolute results obtained using the value $f_{\mathrm{b-baryon}}/f_d = 0.56^{+0.28}_{-0.21}$ extracted from a CDF Run II analysis [15]:

$$\mathcal{B}(\Lambda_b^0 \to p\pi^-) = (1.4 \pm 0.3\ (stat.)^{+0.9}_{-0.5}\ (syst.)) \times 10^{-6},$$

$$\mathcal{B}(\Lambda_b^0 \to pK^-) = (2.2 \pm 0.3\ (stat.)^{+1.4}_{-0.8}\ (syst.)) \times 10^{-6}.$$

All absolute results are in agreement with Standard Model expectations and exclude $O(10^{-4})$ values indicated for R-parity violating Minimal Supersymmetric extensions of the Standard Model [2].
With the full Run II statistics, assuming no improvements in the analysis and a similar trigger efficiency, we expect $\mathcal{O}(7\%)$ statistical uncertainty on the asymmetry and $\mathcal{O}(0.003)$ statistical uncertainty on the relative branching fractions.

Acknowledgments

We thank the Fermilab staff and the technical staffs of the participating institutions for their vital contributions. This work was supported by the U.S. Department of Energy and National Science Foundation; the Italian Istituto Nazionale di Fisica Nucleare; the Ministry of Education, Culture, Sports, Science and Technology of Japan; the Natural Sciences and Engineering Research Council of Canada; the National Science Council of the Republic of China; the Swiss National Science Foundation; the A.P. Sloan Foundation; the Bundesministerium für Bildung und Forschung, Germany; the Korean Science and Engineering Foundation and the Korean Research Foundation; the Science and Technology Facilities Council and the Royal Society, UK; the Institut National de Physique Nucleaire et Physique des Particules/CNRS; the Russian Foundation for Basic Research; the Comisión Interministerial de Ciencia y Tecnología, Spain; the European Community's Human Potential Programme; the Slovak R&D Agency; and the Academy of Finland.

[1] R. Mohanta, A. K. Giri, and M. P. Khanna, Phys. Rev. **D63**, 074001 (2001).
[2] R. Mohanta, Phys. Rev. **D63**, 056006 (2001).
[3] R. Blair *et al.* (CDF Collaboration) The CDF II Detector Technical Design Report, FERMILAB-PUB-96/390-E; A. Sill *et al.* Nucl. Instrum. Meth. **A447**, 1 (2000); T. Affolder *et al.* Nucl. Instrum. Meth. **A526**, 249 (2004).
[4] D. Acosta *et al.* (CDF Collaboration), Phys. Rev. **D72**, 051104 (2005).
[5] CDF Collaboration, public Note 8464 (2006) linked at `www-cdf.fnal.gov/physics/new/bottom/060921.blessed-bhh_1fb`; M. Morello Ph.D. Thesis, Scuola Normale Superiore, Pisa (in preparation).
[6] G. Volpi, Ph.D. Thesis, Siena University, Siena (in preparation).
[7] CDF II uses a cylindrical coordinate system in which ϕ is the azimuthal angle, r is the radius from the nominal beam line, and z points in the proton beam direction, with the origin at the center of the detector. The transverse plane is the plane perpendicular to the z axis.
[8] W. J. Ashmanskas *et al.*, Nucl. Instrum. Meth. **A518**, 532 (2004).
[9] G. Punzi, eConf **C030908**, MODT002 (2003) [arXiv:physics/0308063].
[10] W.-M. Yao *et al.* (Particle Data Group), J. Phys. G **33**, 1 (2006) and web update 2007: `http://pdg.lbl.gov`.
[11] V. Cirigliano, J. F. Donoghue, and E. Golowich, Eur. Phys. J. C **18**, 83 (2000); E. Baracchini and G. Isidori, Phys. Lett. B **633**, 309 (2006).
[12] D. Acosta *et al.* (CDF Collaboration), Phys. Rev. Lett. **96**, 202001 (2006).
[13] D. Tonelli, Ph.D. Thesis, Scuola Normale Superiore, Pisa; FERMILAB-THESIS-2006-23 (2006).
[14] A. Abulencia *et al.* (CDF Collaboration), Phys. Rev. Lett. **96**, 202001 (2006).
[15] CDF Collaboration, public Note 8140 (2006), linked at `www-cdf.fnal.gov/physics/new/bottom/060216.blessed-fqFractions/`.
[16] A. Abulencia *et al.* (CDF Collaboration), Phys. Rev. Lett. **98**, 122002 (2007)

VIII. TABLES

Track variable	Trigger cut value	Offline cut value
$\mid \eta \mid$	≤ 1.2	≤ 1
p_T	≥ 2 GeV/c	≥ 2 GeV/c
$p_T(1) + p_T(2)$	≥ 5.5 GeV/c	≥ 5.5 GeV/c
$q(1) \cdot q(2)$	< 0	< 0
Azimuthal opening angle	$20^\circ < \Delta\phi < 135^\circ$	$20^\circ < \Delta\phi < 135^\circ$
Impact parameter	$0.1 \leq \lvert d_0 \rvert \leq 1$ mm	$0.1 \leq \lvert d_0 \rvert \leq 1$ mm
$d_0(1) \cdot d_0(2)$	–	<0 cm^2
Drift chamber axial layers	–	≥ 2 (w/ ≥ 4 hits each)
Drift chamber stereo layers	–	≥ 2 (w/ ≥ 5 hits each)
Axial silicon information	–	≥ 3 hits
Tracking algorithm	–	axial or stereo silicon hits
Candidate variable		
$\mid \eta(B) \mid$	–	≤ 1
$\mid d_0(B) \mid$	≤ 140 μm	≤ 60 μm
$\mid L_{xy}(B) \mid$	≥ 200 μm	≥ 350 μm
Invariant mass	$4 \leq m_{\pi\pi} \leq 7$ GeV/c^2	–
Vertex fit quality	–	$\chi^2_{3D} \leq 5$
Isolation	–	$I_{R=1}(B) \geq 0.525$
$p_{\mathrm{T}}(B)$	–	≥ 6 GeV/c

TABLE I: Trigger confirmation and final offline cuts applied to the tracks and to the $B^0_{(s)} \to h^+h^{'-}$ candidate.

Parameter	Estimated fraction	Estimated yield
$B^0 \to \pi^+\pi^-$ + c.c.	0.149 ± 0.010	625 ± 40
$B^0 \to K^+\pi^-$ + c.c.	0.574 ± 0.013	2398 ± 56
$A_{\mathsf{CP}}(B^0 \to K^+\pi^-)$	-0.077 ± 0.028	–
$B^0_s \to K^-\pi^+$ + c.c.	0.034 ± 0.006	142 ± 27
$A_{\mathsf{CP}}(B^0_s \to K^-\pi^+)$	0.22 ± 0.19	–
$B^0_s \to K^+K^-$ + c.c.	0.182 ± 0.010	760 ± 41
$B^0_s \to \pi^+\pi^-$ + c.c.	0.004 ± 0.003	17 ± 13
$B^0 \to K^+K^-$ + c.c.	0.011 ± 0.005	45 ± 20
$\Lambda^0_b \to pK^-$ + c.c.	0.028 ± 0.004	116 ± 15
$A_{\mathsf{CP}}(\Lambda^0_b \to pK^-)$	0.37 ± 0.17	–
$\Lambda^0_b \to p\pi^-$ + c.c.	0.019 ± 0.003	78 ± 14
$A_{\mathsf{CP}}(\Lambda^0_b \to p\pi^-)$	0.01 ± 0.17	–

TABLE II: Raw physics results from the fit. By 'raw" we mean that the numbers have not been corrected for the relative efficiency factors.

Parameter	Estimate
f_{π^+} (combinatorial)	0.536 $\pm$ 0.066
f_{e^+} (combinatorial)	0.085 $\pm$ 0.028
f_p (combinatorial)	0.079 $\pm$ 0.087
f_{K^+} (combinatorial)	0.299 $\pm$ 0.119
f_{π^-} (combinatorial)	0.583 $\pm$ 0.064
f_{e^-} (combinatorial)	0.056 $\pm$ 0.026
$f_{\bar{p}}$ (combinatorial)	0.173 $\pm$ 0.102
f_{K^-} (combinatorial)	0.188 $\pm$ 0.127
fraction of physics bckg (ARGUS norm.)	0.673 $\pm$ 0.034
ARGUS cut-off [GeV/c^2]	5.149 $\pm$ 0.001
ARGUS shape	4.528 $\pm$ 2.76
background fraction	0.249 $\pm$ 0.008
c_1 (background shape)	-0.130 $\pm$ 0.043

TABLE III: Results for other fit parameters.

Source	$A_{\mathsf{CP}}(\Lambda_b^0 \to pK^-)$	$A_{\mathsf{CP}}(\Lambda_b^0 \to p\pi^-)$	$\frac{\sigma(p\bar{p}\to\Lambda_b^0 X)}{\sigma(p\bar{p}\to B^0 X)}\frac{\mathcal{B}(\Lambda_b^0\to pK^-)}{\mathcal{B}(B^0\to K^+\pi^-)}$	$\frac{\sigma(p\bar{p}\to\Lambda_b^0 X)}{\sigma(p\bar{p}\to B^0 X)}\frac{\mathcal{B}(\Lambda_b^0\to p\pi^-)}{\mathcal{B}(B^0\to K^+\pi^-)}$
Mass scale	0.004	0.017	0.0014	0.0022
Input masses	0.011	0.041	0.0016	0.0013
dE/dx	0.022	0.014	0.0030	0.0014
Comb. bckg	0.001	0.004	0	0.0003
Polarization	0.004	0.002	0.0009	0.0005
Charge asymm.	0.008	0.024	-	-
Lifetime	-	-	0.0001	0.0004
$p_{\mathrm{T}}(\Lambda_b^0)$	< 0.001	0.003	0.0005	0.0019
Isolation eff.	-	-	0.0066	0.0042
Track trigger eff	-	-	0.0033	0.0021
Total	0.026	0.053	0.0084	0.0058

TABLE IV: Systematic uncertainties. The total is determined as the sum in quadrature of single contributions.

IX. FIGURES

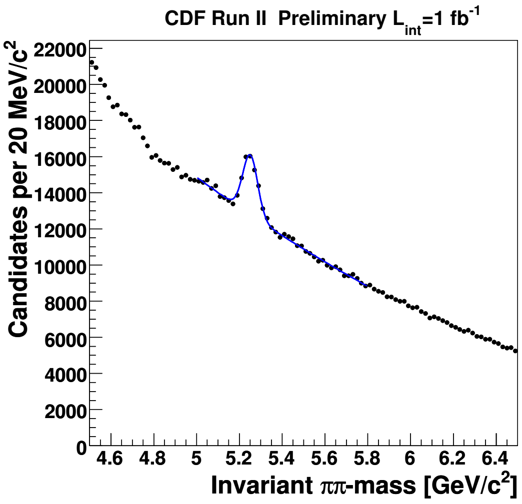

FIG. 1: Invariant $\pi\pi$-mass distribution obtained after applying only the trigger confirmation cuts. A Gaussian (signal) plus exponential (background) fit function is overlaid.

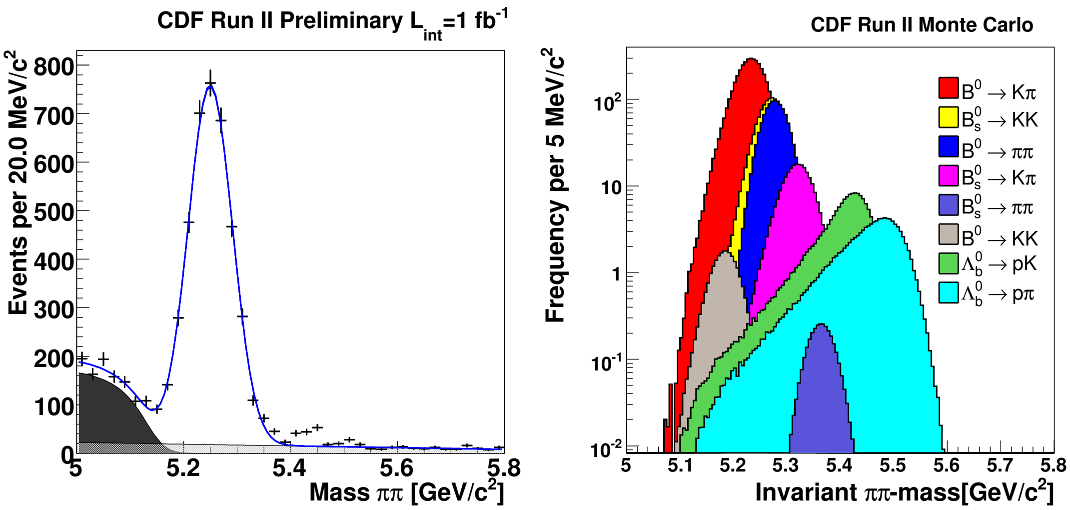

FIG. 2: Invariant $\pi\pi$-mass distribution resulting from the selection of table I (left plot). A Gaussian (signal) plus exponential (combinatoric background) plus a smeared Argus (physical background) fit function is overlaid. The mass region $5.38 < m_{\pi\pi} < 5.52$ GeV/c^2, where contributions from three new modes ($B_s^0 \to K^-\pi^+$, $\Lambda_b^0 \to p\pi^-$, $\Lambda_b^0 \to pK^-$) is expected, is excluded. Invariant $\pi\pi$-mass of simulated $B^0_{(s)} \to h^+h^{'-}$ signals. The relative contributions are based on measured branching fractions of the already observed modes ($B^0 \to \pi^+\pi^-$, $B^0 \to K^+\pi^-$ $B_s^0 \to K^+K^-$) and on theoretically-expected values for the unobserved modes ($B^0 \to K^+K^-$, $B_s^0 \to K^-\pi^+$, $B_s^0 \to \pi^+\pi^-$, $\Lambda_b^0 \to p\pi^-$, $\Lambda_b^0 \to pK^-$) (right plot).

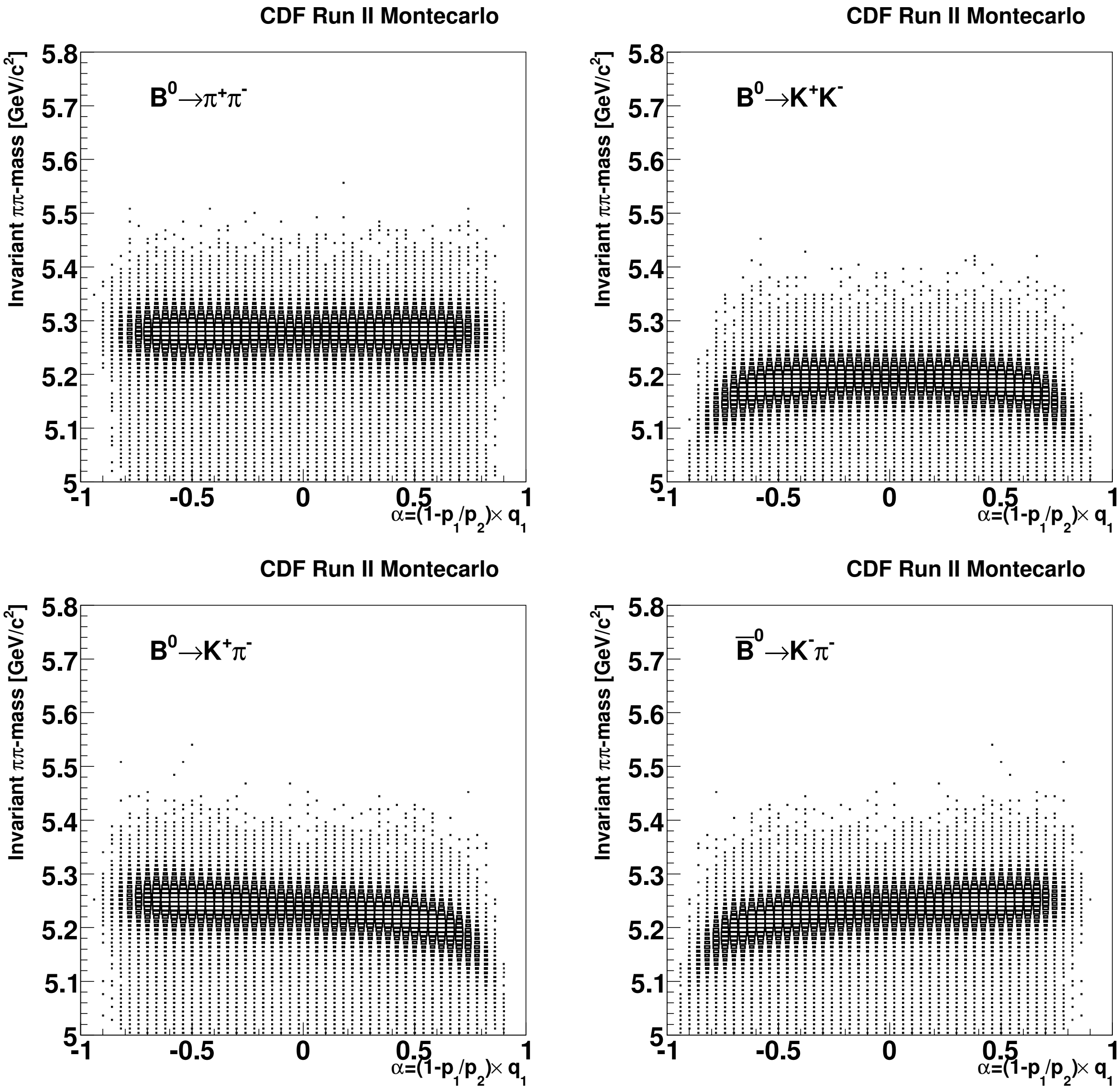

FIG. 3: Invariant $m_{\pi\pi}$ distribution of simulated $B^0 \to \pi^+\pi^-$, $B^0 \to K^+K^-$, $B^0 \to K^+\pi^-$, $\overline{B}^0 \to K^-\pi^+$ signals as a function of α. Effect of final state radiation is simulated.

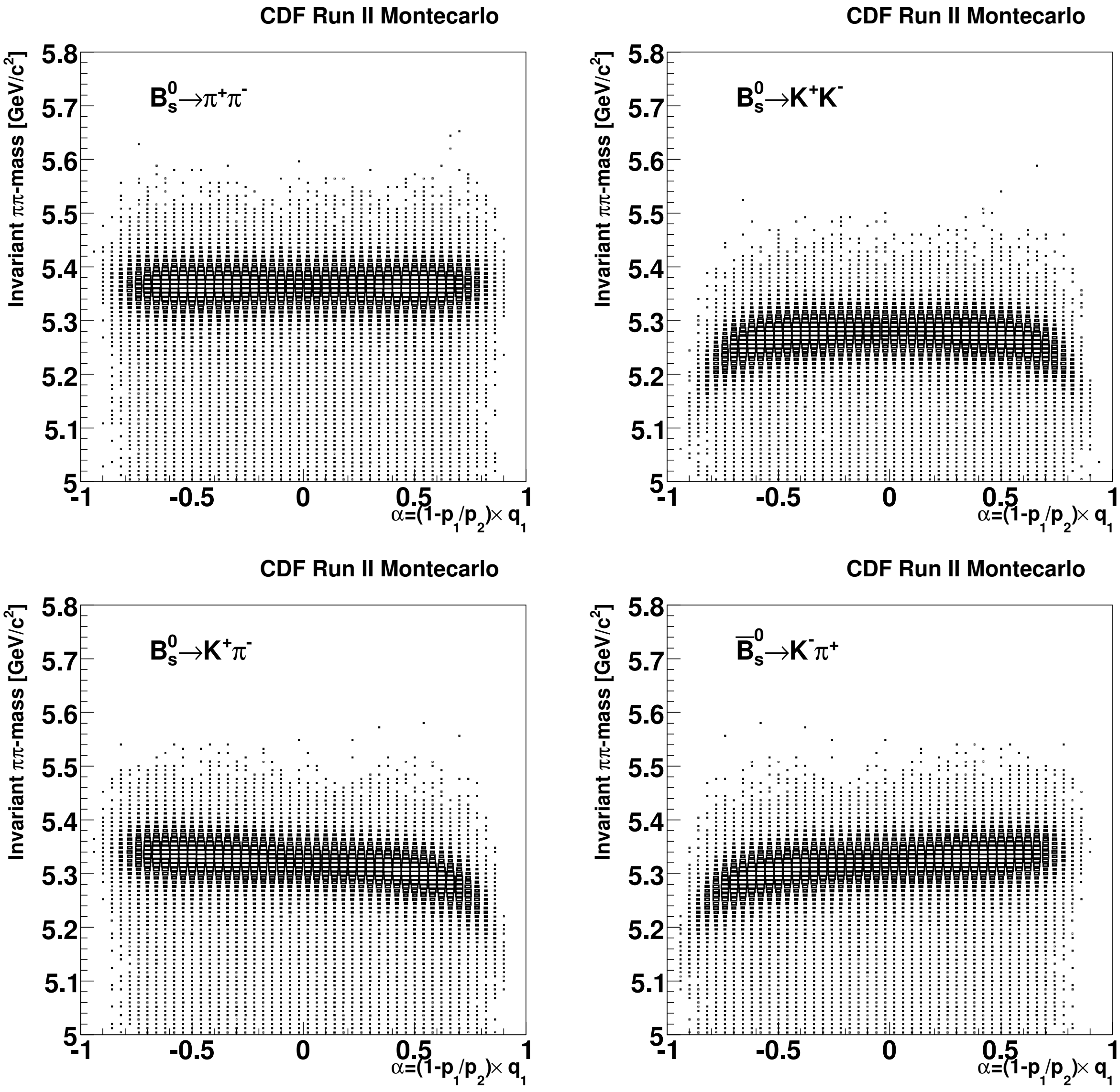

FIG. 4: Invariant $m_{\pi\pi}$ distribution of simulated $B_s^0 \to \pi^+\pi^-$, $B_s^0 \to K^+K^-$, $B_s^0 \to K^-\pi^+$, $\overline{B}_s^0 \to K^+\pi^-$ signals as a function of α. Effect of final state radiation is simulated.

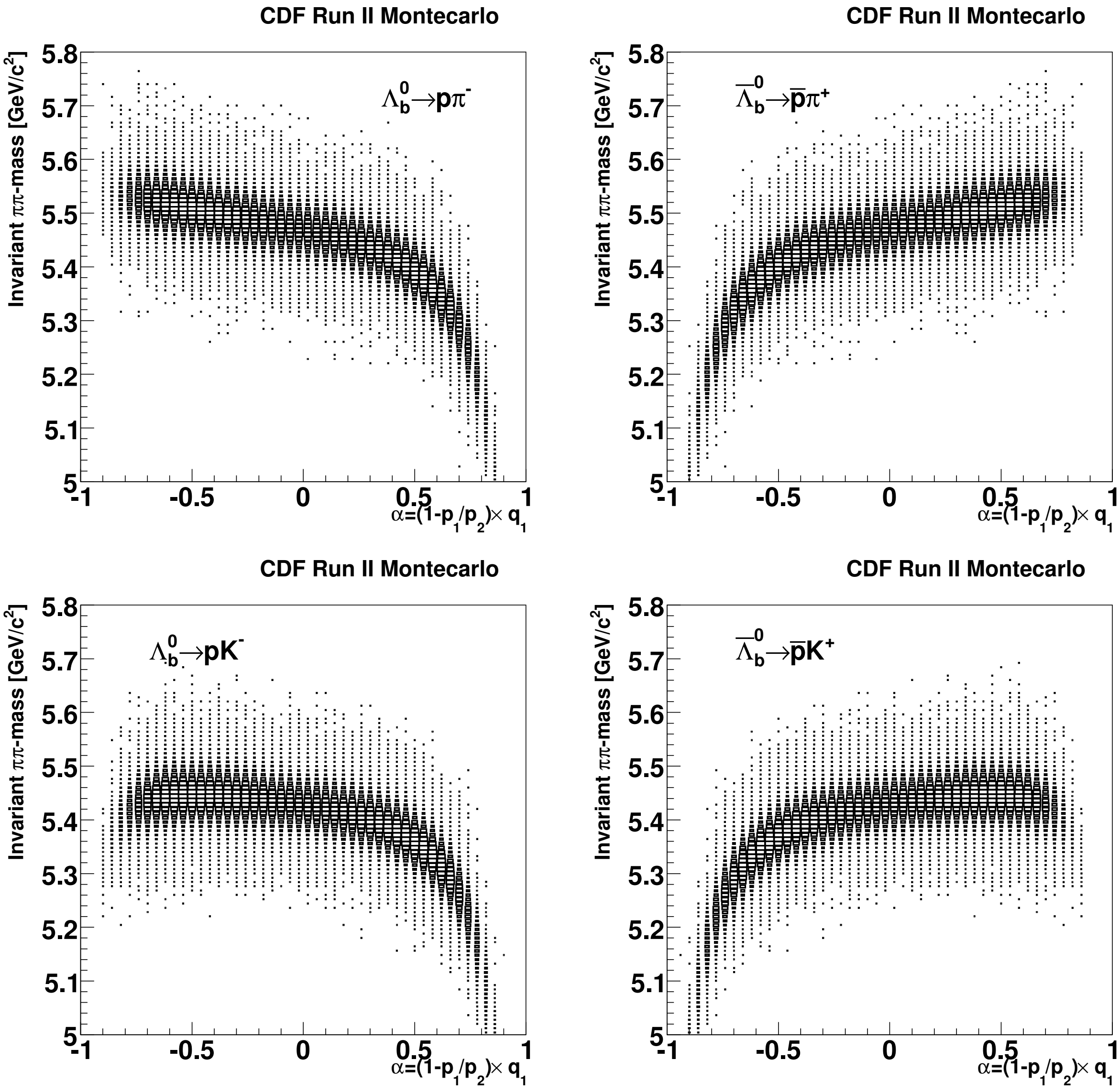

FIG. 5: Invariant $m_{\pi\pi}$ distribution of simulated $\Lambda_b^0 \to p\pi^-$, $\overline{\Lambda}_b^0 \to \overline{p}\pi^+$, $\Lambda_b^0 \to pK^-$, $\overline{\Lambda}_b^0 \to \overline{p}K^+$ signals as a function of α.

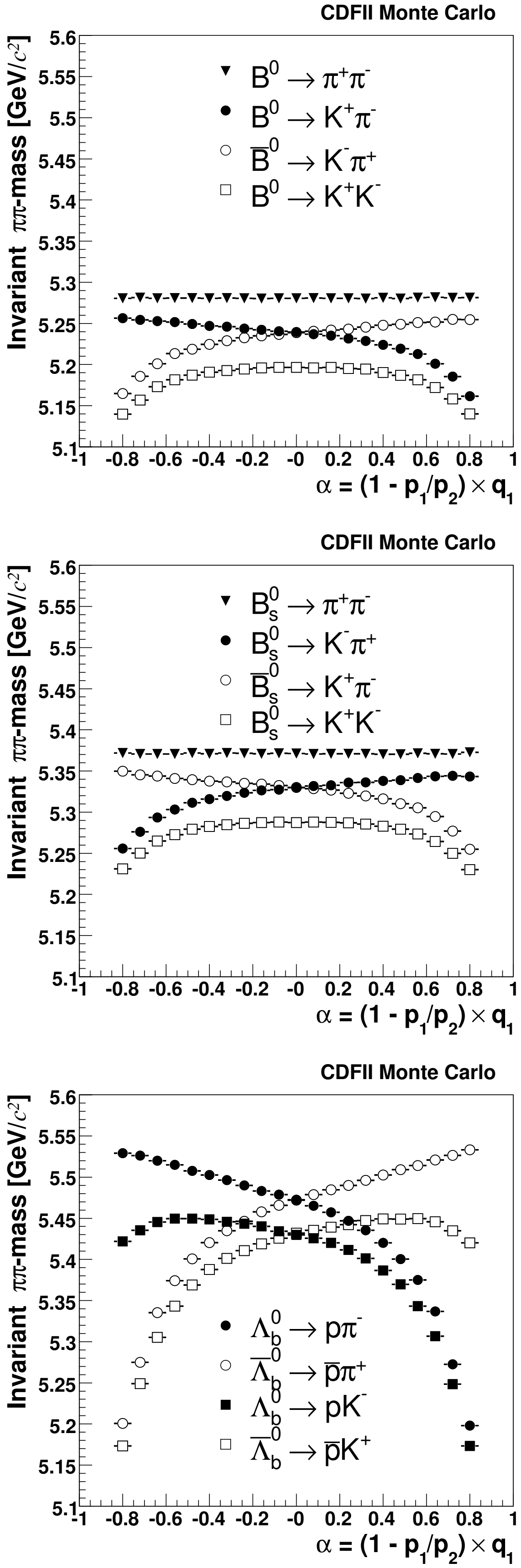

FIG. 6: Averaged $m_{\pi\pi}$ distribution of $B^0_{(s)} \to h^+h^{'-}$ and $\Lambda_b^0 \to ph^-$ simulated signals as a function of α.

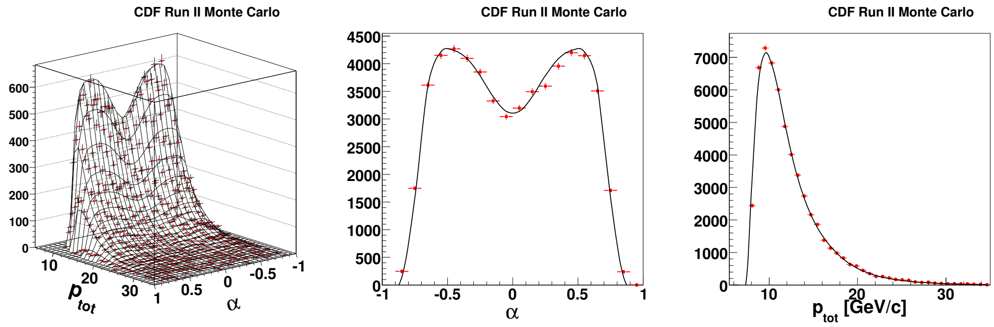

FIG. 7: Joint $(\alpha, p_{\rm tot})$ density for the mode $B^0 \to \pi^+\pi^-$. Left plot shows the two-dimensional fit overlaid to the distribution of Monte Carlo data. The other two plots show the projections of the parameterization in the α and $p_{\rm tot}$ axis.

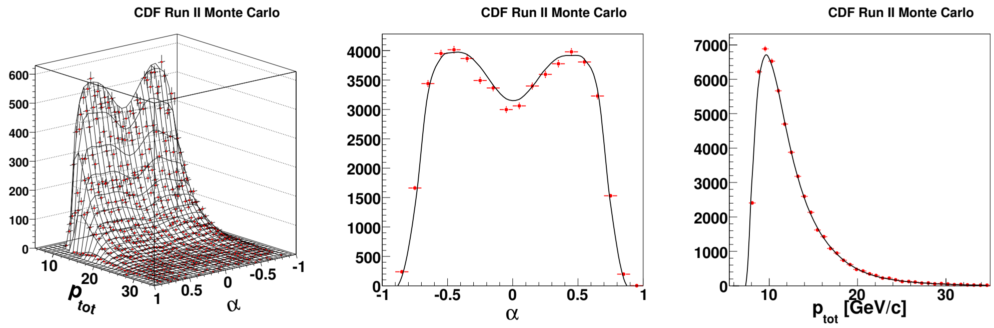

FIG. 8: Joint $(\alpha, p_{\rm tot})$ density for the mode $B^0 \to K^+\pi^-$. Left plot shows the two-dimensional fit overlaid to the distribution of Monte Carlo data. The other two plots show the projections of the parameterization in the α and $p_{\rm tot}$ axis.

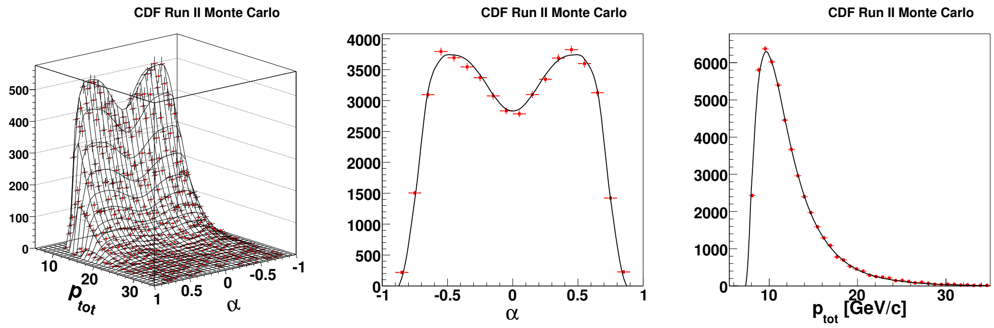

FIG. 9: Joint $(\alpha, p_{\rm tot})$ density for the mode $B^0 \to K^+K^-$. Left plot shows the two-dimensional fit overlaid to the distribution of Monte Carlo data. The other two plots show the projections of the parameterization in the α and $p_{\rm tot}$ axis.

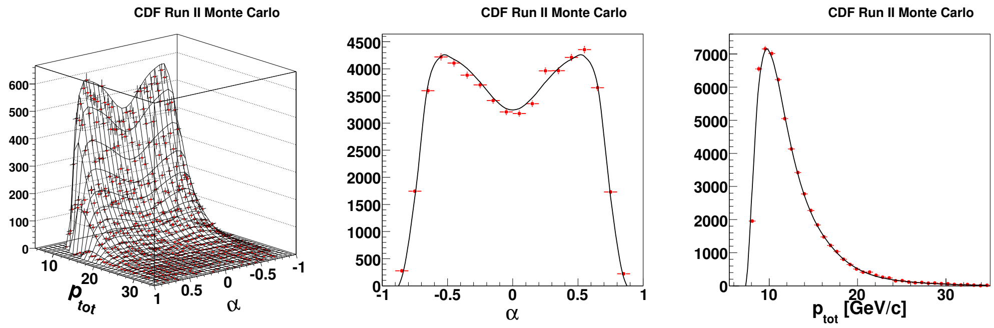

FIG. 10: Joint $(\alpha, p_{\rm tot})$ density for the mode $B_s^0 \to \pi^+\pi^-$. Left plot shows the two-dimensional fit overlaid to the distribution of Monte Carlo data. The other two plots show the projections of the parameterization in the α and $p_{\rm tot}$ axis.

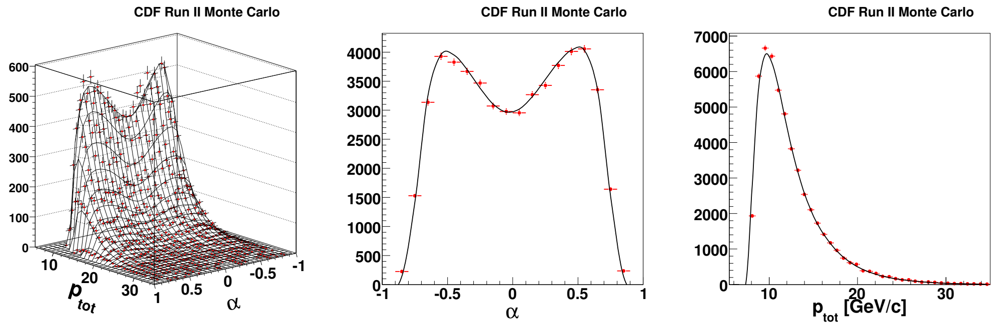

FIG. 11: Joint $(\alpha, p_{\rm tot})$ density for the mode $B_s^0 \to K^-\pi^+$. Left plot shows the two-dimensional fit overlaid to the distribution of Monte Carlo data. The other two plots show the projections of the parameterization in the α and $p_{\rm tot}$ axis.

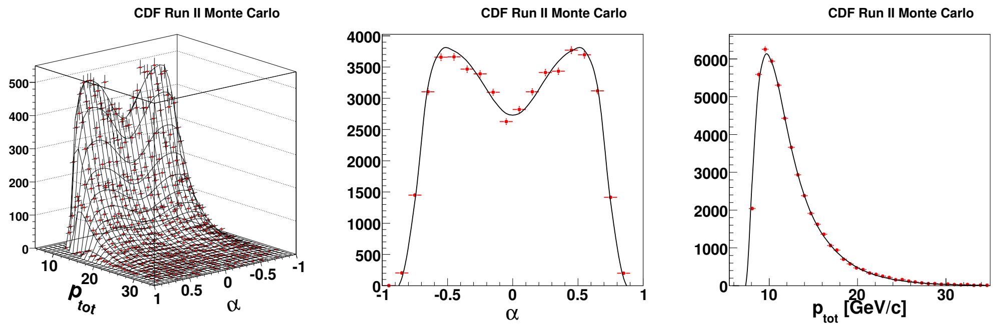

FIG. 12: Joint $(\alpha, p_{\rm tot})$ density for the mode $B_s^0 \to K^+K^-$. Left plot shows the two-dimensional fit overlaid to the distribution of Monte Carlo data. The other two plots show the projections of the parameterization in the α and $p_{\rm tot}$ axis.

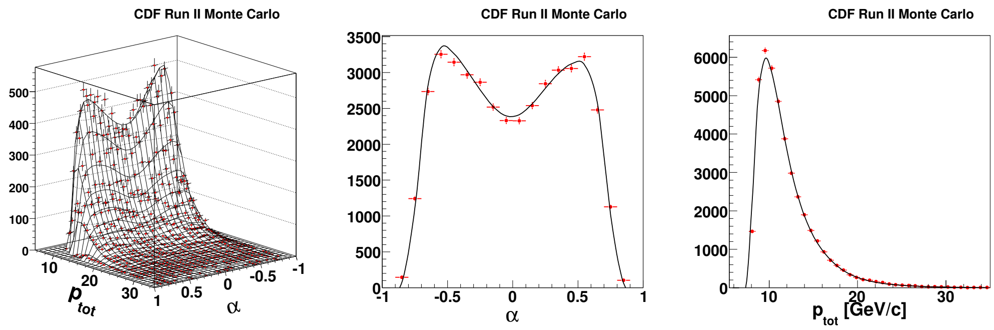

FIG. 13: Joint $(\alpha, p_{\rm tot})$ density for the mode $\Lambda_b^0 \to p\pi^-$. Left plot shows the two-dimensional fit overlaid to the distribution of Monte Carlo data. The other two plots show the projections of the parameterization in the α and $p_{\rm tot}$ axis.

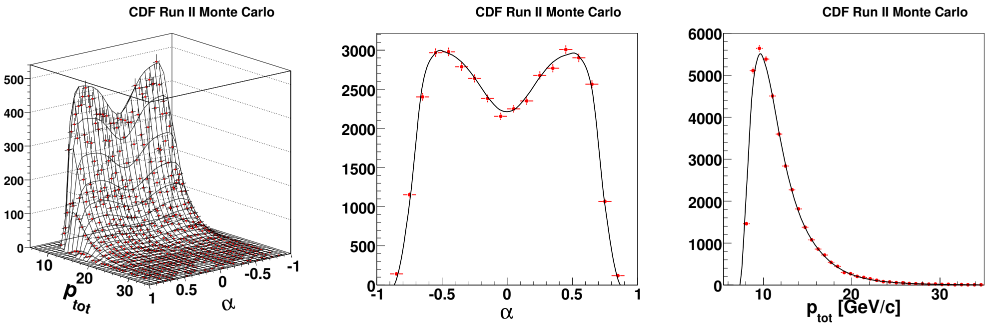

FIG. 14: Joint $(\alpha, p_{\rm tot})$ density for the mode $\Lambda_b^0 \to pK^-$. Left plot shows the two-dimensional fit overlaid to the distribution of Monte Carlo data. The other two plots show the projections of the parameterization in the α and $p_{\rm tot}$ axis.

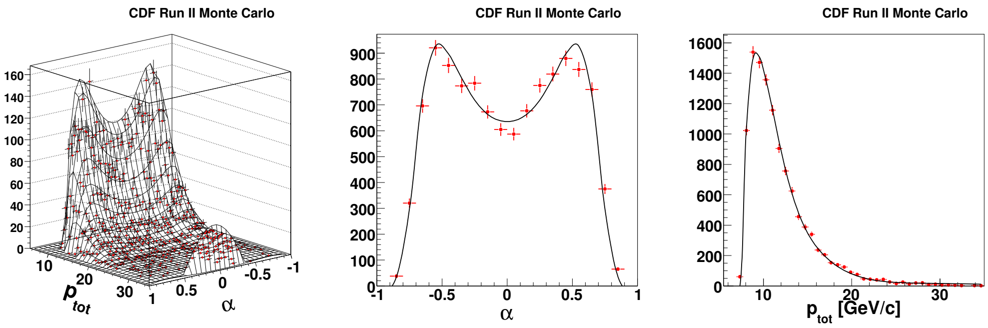

FIG. 15: Joint $(\alpha, p_{\rm tot})$ density for the mode multi-body decays. Left plot shows the two-dimensional fit overlaid to the distribution of Monte Carlo data. The other two plots show the projections of the parameterization in the α and $p_{\rm tot}$ axis.

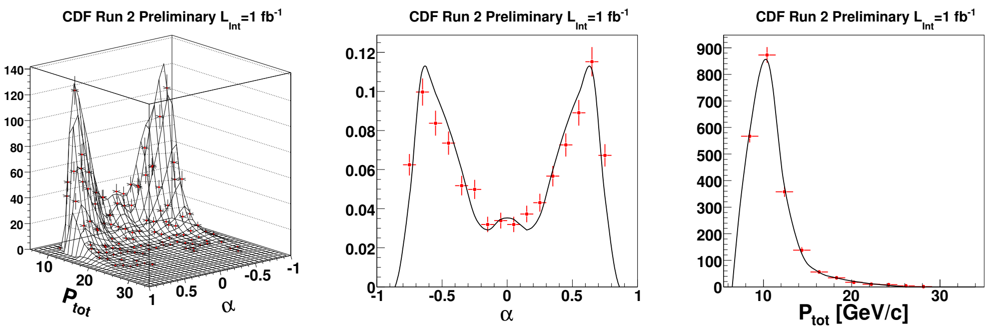

FIG. 16: Joint $(\alpha, p_{\rm tot})$ density for the combinatoric background. Left plot shows the two-dimensional fit overlaid to the distribution of real data with $m_{\pi\pi} > 5.6$ MeV$/c^2$. The other two plots show the projections of the parameterization in the α and $p_{\rm tot}$ axis.

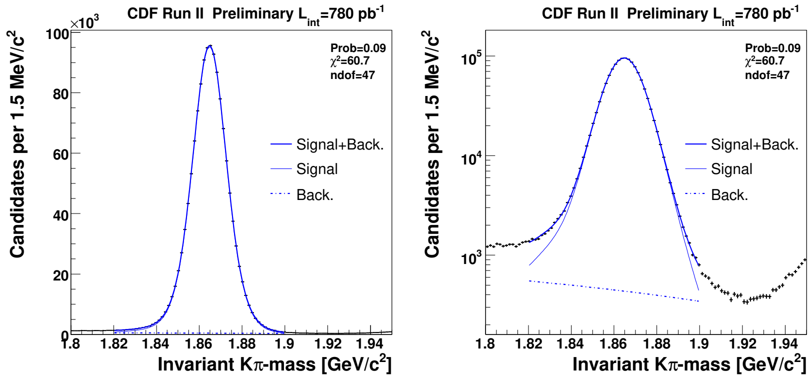

FIG. 17: Check of the mass line shape template using D^0 mass $D^{*+} \to D^0(\to K^-\pi^+)\pi^+$. The blue line is the result of a fit where the signal line shape is completely fixed from the model.

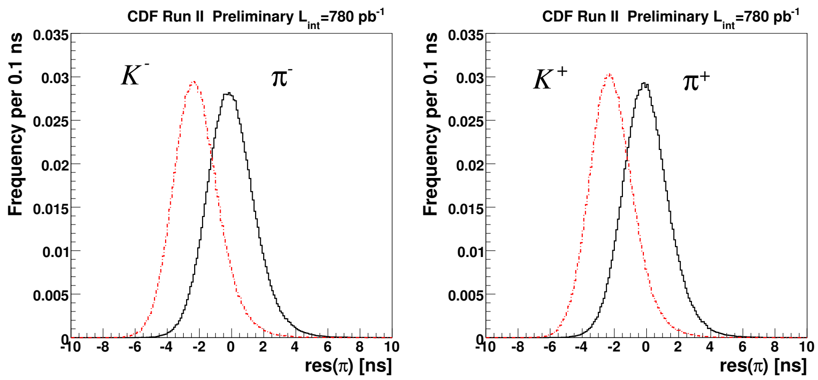

FIG. 18: Distribution of dE/dx around the average pion response, for calibration samples of negative (left plot) and positive (right plot) kaons and pions from $D^{*+} \to D^0(\to K^-\pi^+)\pi^+$ decays.

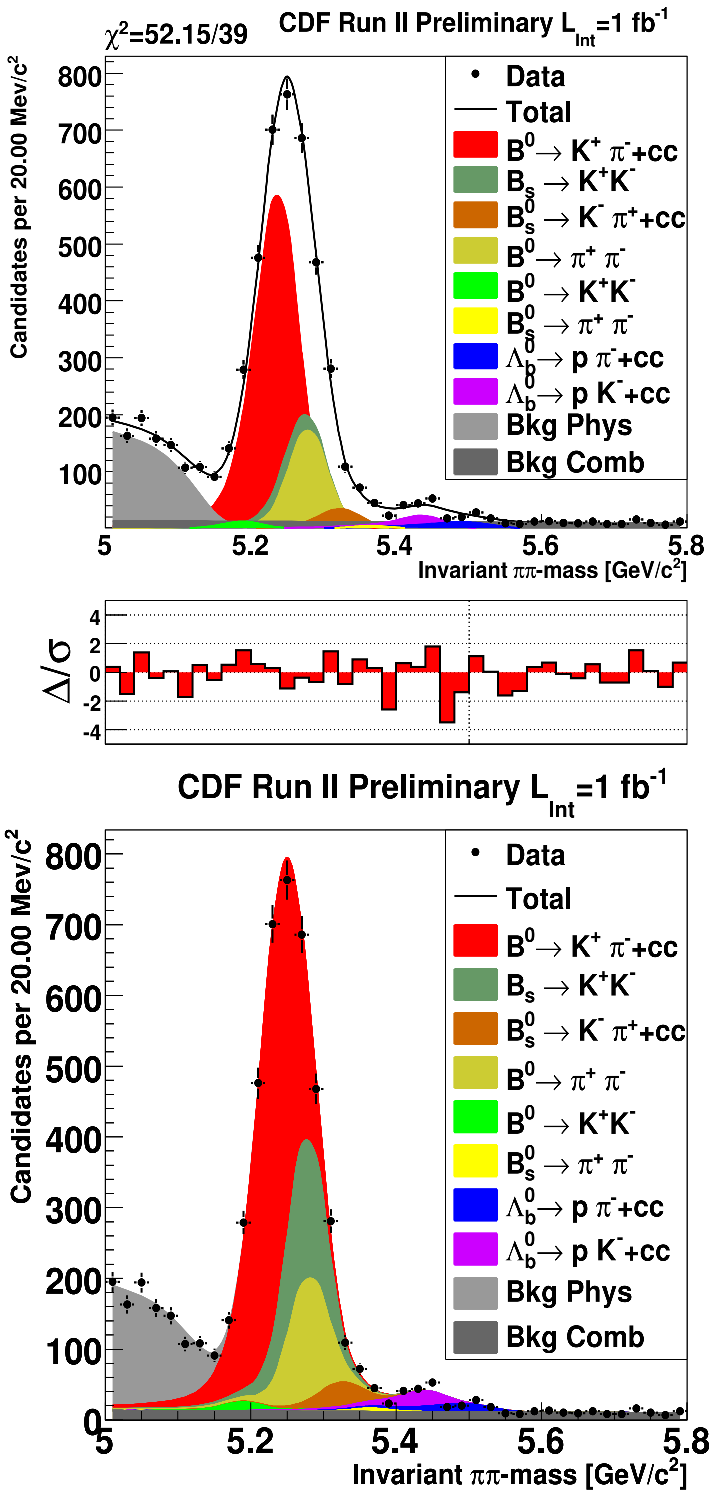

FIG. 19: Fit projection in the whole mass range onto the $m_{\pi\pi}$ variable.

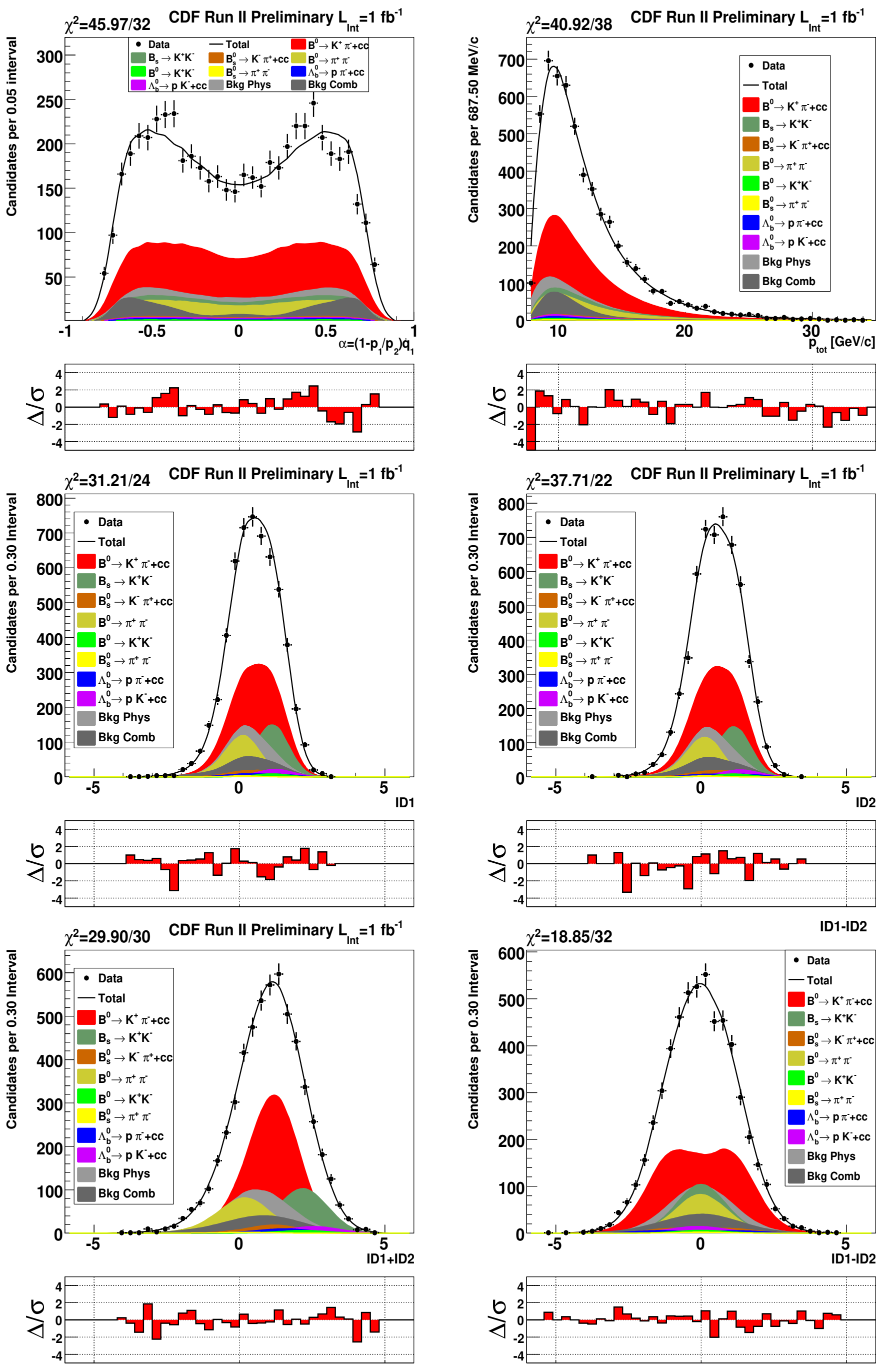

FIG. 20: Fit projections in the whole mass range onto the α, $p_{\rm tot}$, $\mathsf{ID}_{\min}$, $\mathsf{ID}_{\max}$, $\mathsf{ID}_{\min}+\mathsf{ID}_{\max}$, $\mathsf{ID}_{\min}-\mathsf{ID}_{\max}$ variables.

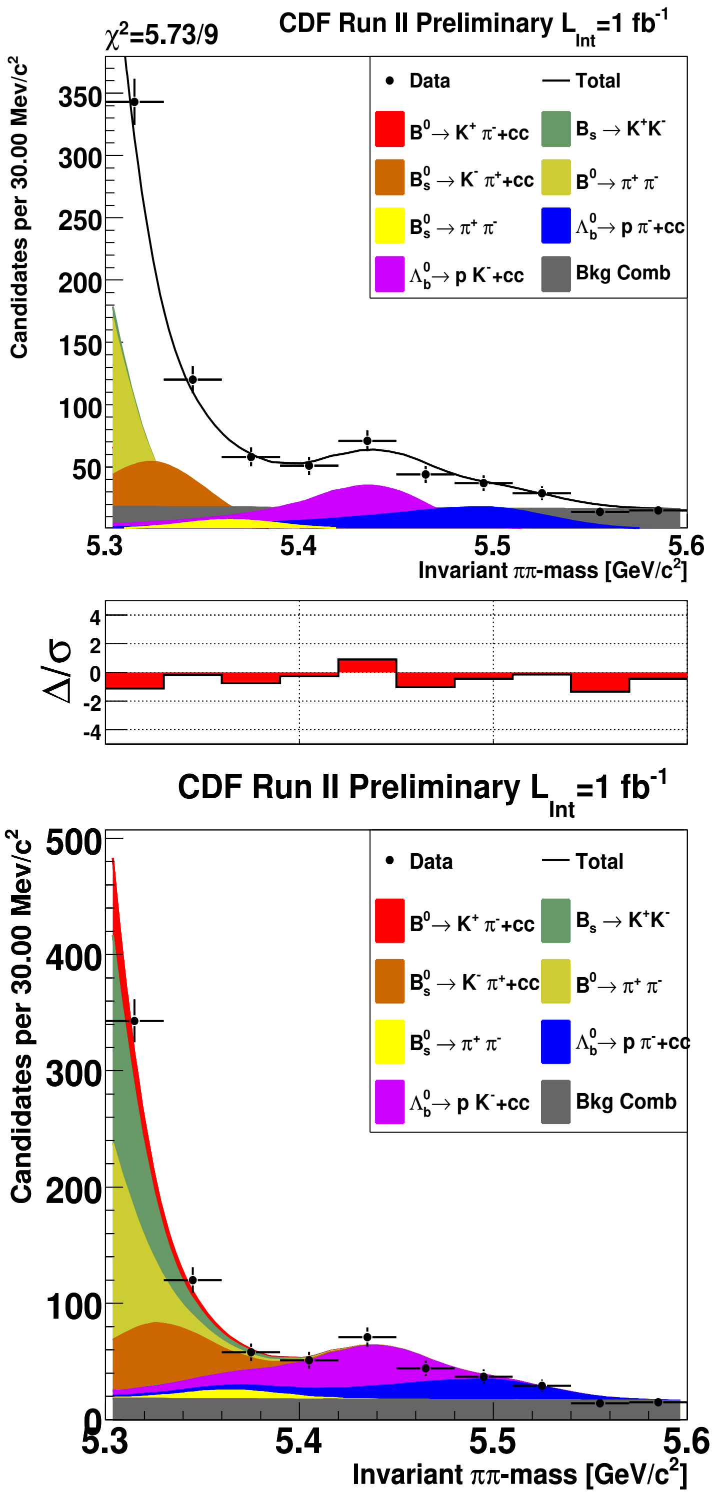

FIG. 21: Fit projection in the Λ_b^0 mass range onto the $m_{\pi\pi}$ variable.

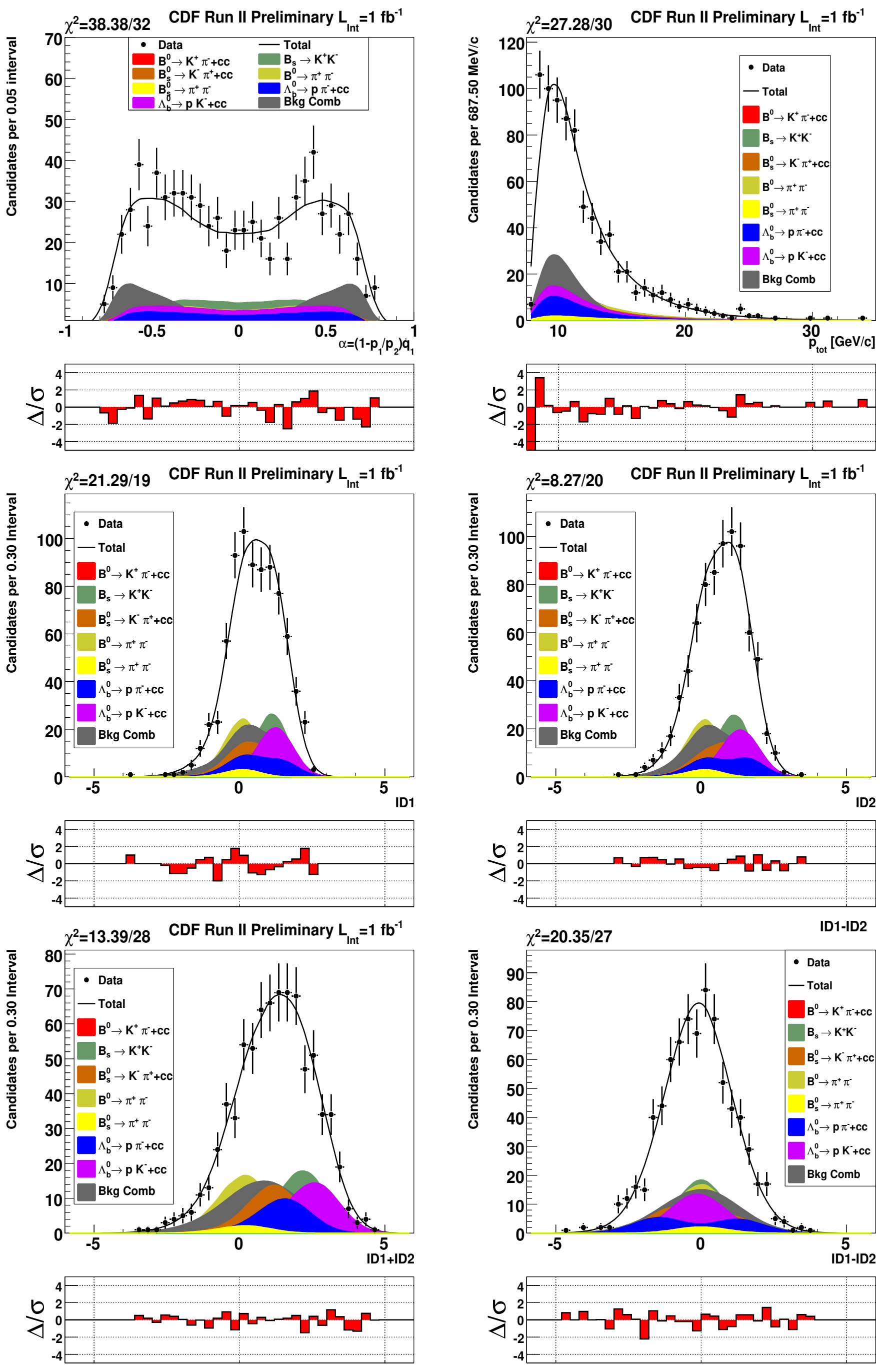

FIG. 22: Fit projections in the Λ_b^0 mass range onto the α, $p_{\rm tot}$, $\mathsf{ID}_{\min}$, $\mathsf{ID}_{\max}$, $\mathsf{ID}_{\min}+\mathsf{ID}_{\max}$, $\mathsf{ID}_{\min}-\mathsf{ID}_{\max}$ variables.

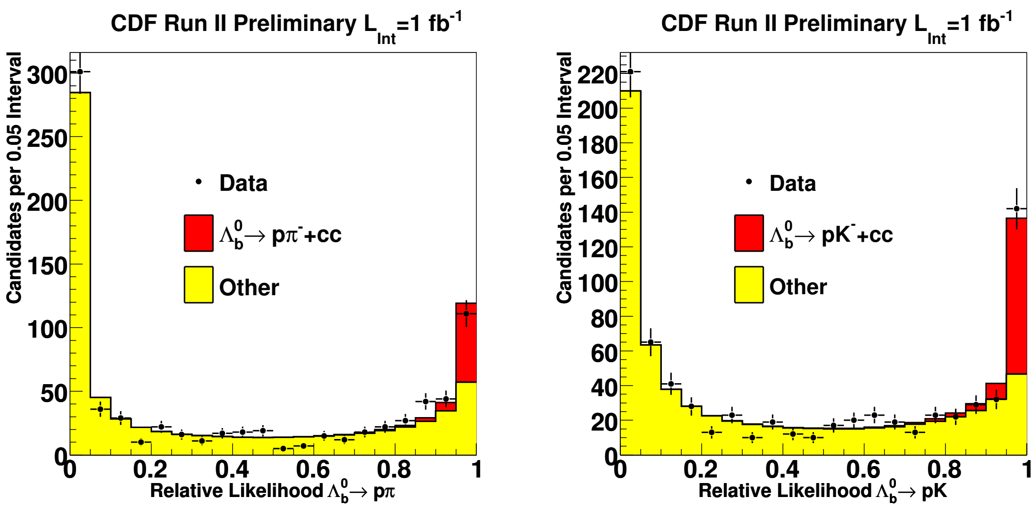

FIG. 23: Relative Likelihood for $\Lambda_b^0 \to p\pi^-$ (left plot) and $\Lambda_b^0 \to pK^-$ (right plot) versus background in the signal mass region ($5.1 < m_{\pi\pi} < 5.6$ GeV/c^2). The relative likelihood is the ratio between the total p.d.f. of the signal and the sum of this one with the background p.d.f. This quantity yields preferably a number closer to one in a true signal event, while yielding a number closer to zero for a background event.

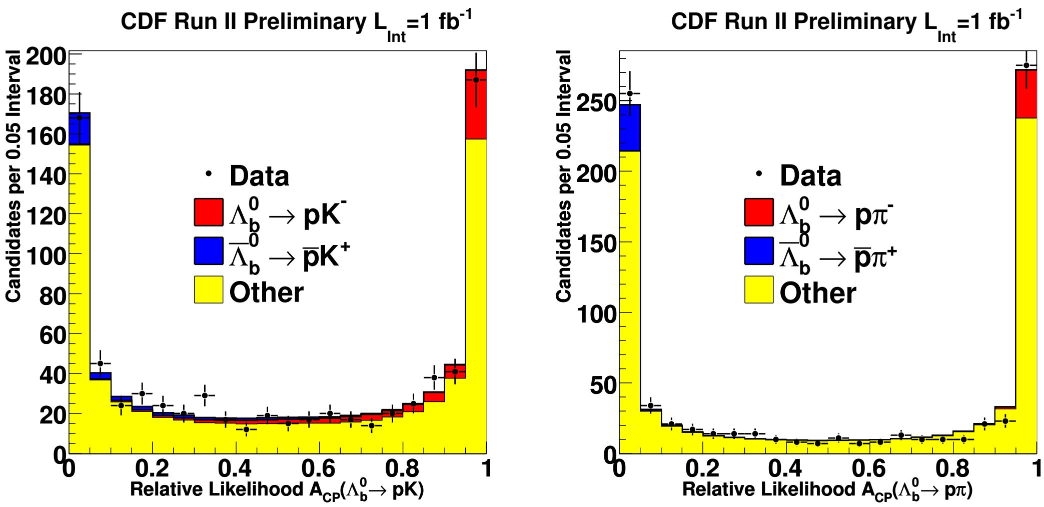

FIG. 24: Relative Likelihood for the CP-violating asymmetries in the signal mass region ($5.1 < m_{\pi\pi} < 5.6$ GeV/c^2). The relative likelihood is the ratio between the total p.d.f. of the signal and the sum of this one with the background p.d.f. This quantity yields preferably a number closer to one in a true signal event, while yielding a number closer to zero for a background event.